Journal of Computational Physics **179,** 426–438 (2002)
doi:10.1006/jcph.2002.7063

# Stability of Explicit–Implicit Hybrid Time-Stepping Schemes for Maxwell's Equations

Thomas Rylander and Anders Bondeson

*Department of Electromagnetics and Center for Computational Electromagnetics, Chalmers University of Technology, S-412 96 Göteborg, Sweden*
E-mail: rylander@elmagn.chalmers.se

Received September 12, 2001; revised March 25, 2002

An improved version of the stable FEM–FDTD hybrid method [T. Rylander and A. Bondeson, *Comput. Phys. Commun.* **125**, 75 (2000)] for Maxwell's equations is presented. The new formulation has a modified time-stepping scheme and is rigorously proven to be stable for time steps up to the stability limit for the FDTD. The new scheme gives less reflection at the boundary between the structured and unstructured grids than the original formulation. The hybrid method is compared to the FDTD, with staircasing for scattering from a conducting sphere. The discretization errors of the hybrid show quadratic dependence on mesh size, while the scaling is less clear for the FDTD. The FDTD gives errors that are 5–60 times higher than that of the hybrid, depending on resolution and staircasing strategy. © 2002 Elsevier Science (USA)

*Key Words:* FEM; FDTD; staircase approximation; explicit–implicit time stepping; hybrid scheme; stability; scattering; Maxwell's equations.

## 1. INTRODUCTION

Each of the two main methods in time-domain computational electromagnetics, the finite-difference time domain (FDTD) [1, 2] and the finite-element method (FEM) [3] with edge elements [4], has advantages and disadvantages. The FDTD is very efficient, because it is explicit and simple. However, it has difficulties with oblique and curved boundaries, where staircasing is the standard solution. Finite elements with tetrahedral grids, on the other hand, are well suited for modeling complex geometry. However, the time stepping is generally implicit and the method has much higher operation count and memory requirement than the FDTD.

Hybrids have been formulated [5–8], with the goal of combining the advantages of the two basic methods. To maximize efficiency, such hybrids use FDTD in as large a volume



0021-9991/02 $35.00

as possible, and finite elements in thin layers near boundaries that do not fit on the FDTD grid. Early versions of FEM–FDTD hybrids [5–7] suffered from instabilities known as late time growth. These instabilities were typically stabilized by means of dissipative schemes for time stepping.

Our hybrid method [8] eliminates the instabilities without recourse to dissipation. The key to stability was to derive the spatial operators for the edges at the interface between the FEM and FDTD regions by FEM techniques. It was noted in [8] that the FDTD scheme can be constructed by FEM techniques; Galerkin's method was applied to edge elements on bricks, and the matrices were "lumped," or, equivalently, calculated by trapezoidal integration. This procedure gives symmetric matrices for the spatial operators even at the FEM–FDTD interface. Symmetric, real matrices have real eigenvalues, and this removes the source of instabilities occurring when the two types of grid are joined by more ad hoc approaches.

A second-order-accurate scheme for general geometry has been introduced by Dridi *et al.* [9] using interpolation points at boundaries. However, Ref. [9] does not prove stability and reciprocity of this scheme, and the simulations shown in [9] are over relatively short time intervals. Reference [10] describes a method using overlapping grids and ficitious points to match solutions in different regions meshed by different structured grids. The approach aims at high accuracy but appears very demanding to apply in complex geometries.

There are other methods related to the FDTD scheme which are stable and combine efficiency with body-conforming capabilities. Weiland and co-workers have investigated stable local refinement and nonorthogonal grids for the FDTD scheme [11, 12]. Gwarek and co-workers have developed the transmission line method (TLM) to treat complex boundaries by cutting cells [13]. However, our FEM–FDTD hybrid method is generally more flexible and it allows for local spatial refinement without reducing the global time step. Such local refinement is useful in resolving small geometric details and rapid variations in the fields.

In the present paper, we present an improved time-stepping algorithm for the hybrid method. The new algorithm incorporates FEM ideas also in the time stepping. The new scheme allows a simple proof of stability. A practical advantage of the new algorithm is that it reduces the reflection at the interface between structured and unstructured grids. Both the new scheme and the stability proof are of a rather general nature and could be applied to similar hybrids for other equations, e.g., in acoustics or solid mechanics. We present several different tests of the new method, comparing it both with the staircased FDTD and with the original version of the hybrid. For scattering by a conducting sphere, the hybrid is clearly superior to the FDTD.

## 2. THE HYBRID METHOD

### 2.1. Spatial Discretization

Our hybrid method uses unstructured layers of tetrahedrons close to complex boundaries, while large volumes are discretized by structured brick elements (typically cubes). The connection between the two types of elements is made by a single layer of pyramids. The pyramids make it possible to expand the solution in edge elements, whose tangential components are continuous everywhere.

Maxwell's equation $\nabla \times \mu^{-1} \nabla \times \vec{E} + \epsilon \partial_t^2 \vec{E} = -\partial_t \vec{J}$ is solved by expanding the electric field in edge elements $\vec{E}(\vec{r}, t) = \sum_i e_i(t) \vec{N}_i(\vec{r})$ and applying Galerkin's method. This gives $\mathbf{Se}(t) + \mathbf{M}\, \partial_t^2 \mathbf{e}(t) = \mathbf{f}(t)$, where the stiffness (or curl–curl) matrix $S_{ij} =$

$\int \mu^{-1} \nabla \times \vec{N}_i \cdot \nabla \times \vec{N}_j \, dv$ is symmetric and positive semidefinite, and the mass (or epsilon) matrix $M_{ij} = \int \epsilon \vec{N}_i \cdot \vec{N}_j \, dv$ is symmetric and positive definite. The FDTD algorithm is also found by this approach, if the mass and stiffness matrices are lumped. This corresponds to applying the trapezoidal rule for the integration over the bricks. The properties of the matrices $\mathbf{S}$ and $\mathbf{M}$ implies that the eigenvalues $\omega^2$, of $\mathbf{Se} = \omega^2 \mathbf{Me}$, are all real and nonnegative. Therefore, it is possible to construct a stable time-stepping algorithm.

### 2.2. Time Stepping

We emphasize that in our hybrid scheme, the switch between FDTD and FEM (which is done by the integration method) is linked to the *finite elements* and not the *edges*, or unknowns. Thus, the edges at the interface are treated as neither regular FEM nor regular FDTD. In the first version of the hybrid [8], the switch of the time-stepping scheme was, however, made on the basis of the edges; edges interior to the structured grid were time stepped explicitly and those belonging to the pyramids or tetrahedrons were time stepped with the implicit algorithm [14]

$$\mathbf{S}\left[\theta \mathbf{e}^{(n+1)} - (2\theta - 1)\mathbf{e}^{(n)} + \theta \mathbf{e}^{(n-1)}\right] + \frac{1}{\Delta t^2} \mathbf{M}\left[\mathbf{e}^{(n+1)} - 2\mathbf{e}^{(n)} + \mathbf{e}^{(n-1)}\right] = 0. \tag{1}$$

The algorithm (1) is stable for arbitrarily large time steps if $\theta \geq 1/4$. An important advantage of the implicit FEM part is that the time step need not be reduced if some tetrahedrons are made very small. This allows for adaptivity and good resolution of small geometrical details with only a modest increase in the computational work.

In the original version of the hybrid, we applied the same implicitness parameter $\theta$ to all the implicit *edges*. Concerning the FDTD, the time stepping for $\vec{E}$, after elimination of $\vec{H}$, is the standard centered finite-difference method (1), with $\theta = 0$ and $\mathbf{S}$ and $\mathbf{M}$ lumped according to trapezoidal integration.

In the *new* version of the hybrid, we assign the implicitness parameter $\theta$ on the basis of *elements* rather than edges. This follows the same idea as the previous successful prescription for the spatial discretization. Thus, the implicitness can be treated as a parameter $\theta_k$ for each element $k = 1, \ldots, K$, where $K$ is the number of elements. We introduce the notation $\mathbf{S}_k$ for the contribution to $\mathbf{S}$ from element $k$, so that $\mathbf{S} = \sum_{k=1}^{K} \mathbf{S}_k$, and analogously for $\mathbf{M}$. The new algorithm, where $\theta$ is assigned to the elements, is

$$\sum_{k=1}^{K} \left( \mathbf{S}_k \left[\theta_k \mathbf{e}^{(n+1)} - (2\theta_k - 1)\mathbf{e}^{(n)} + \theta_k \mathbf{e}^{(n-1)}\right] + \frac{1}{\Delta t^2} \mathbf{M}_k \left[\mathbf{e}^{(n+1)} - 2\mathbf{e}^{(n)} + \mathbf{e}^{(n-1)}\right] \right) = 0, \tag{2}$$

where $\theta_k$ is chosen $\geq 1/4$ on the implicit elements and zero on the bricks. As will be shown, this not only reduces reflections at the interface, it also makes possible a simple proof of stability.

### 2.3. Proof of Stability

Here, we prove stability assuming, for simplicity, that $\epsilon$ and $\mu$ are constant. The proof relies on bounds for a quadratic form, and first we need the corresponding result for the FDTD part.

2.3.1. *Eigenvalues of the FDTD for a One-Brick Element*

To bound the quadratic form, we wish to find bounds for the 12 eigenvalues of the FDTD matrices for a single element

$$\mathbf{S}_k\mathbf{e} = \lambda\mathbf{M}_k\mathbf{e} \tag{3}$$

with $\mathbf{S}_k$ and $\mathbf{M}_k$ lumped. Here, seven eigenvalues are exactly zero. These correspond to the "potential modes" $\vec{E} = -\nabla\phi$, where the potential $\phi$ is a trilinear function. The potential can be set to zero at one node, and then there is one eigenmode of (3), with $\lambda = 0$ for each of the remaining seven nodes. To determine the remaining five eigenvalues, we studied the eigenvalue problem (3) using Mathematica for a brick with sides $h_x$, $h_y$, and $h_z$ in the three coordinate directions. We found the remaining eigenvalues to be

$$\lambda_8 = \frac{4}{\epsilon\mu}\left(\frac{1}{h_y^2} + \frac{1}{h_z^2}\right), \quad \lambda_9 = \frac{4}{\epsilon\mu}\left(\frac{1}{h_x^2} + \frac{1}{h_z^2}\right), \quad \lambda_{10} = \frac{4}{\epsilon\mu}\left(\frac{1}{h_x^2} + \frac{1}{h_y^2}\right),$$

and the largest eigenvalue is the pair

$$\lambda_{11} = \lambda_{12} = \frac{4}{\epsilon\mu}\left(\frac{1}{h_x^2} + \frac{1}{h_y^2} + \frac{1}{h_z^2}\right) \equiv \lambda_{\max}. \tag{4}$$

As expected, the largest eigenvalues equal the eigenvalue for the fastest varying exponential function $\exp[j\pi(x/h_x + y/h_y + z/h_z)]$ on a uniform, infinite grid. This mode gives the Courant–Friedrichs–Levy (CFL) limit for the FDTD time step

$$\Delta t \le \Delta t_{\mathrm{CFL}} = 2/\sqrt{\lambda_{\max}}. \tag{5}$$

If $h_x = h_y = h_z = h$, (5) gives the usual CFL limit, $h/c\sqrt{3}$. The explicit expression (4) for the largest eigenvalues gives the inequality, valid for any complex vector $\mathbf{e}$, of

$$\mathbf{e}^H\mathbf{S}_k\mathbf{e} \le \lambda_{\max}\mathbf{e}^H\mathbf{M}_k\mathbf{e}, \tag{6}$$

where $\mathbf{e}^H$ is the complex transpose of $\mathbf{e}$.

2.3.2. *Quadratic Form for the Hybrid Algorithm*

We are now in a position to prove stability by the von Neumann method. Let $\tilde{\mathbf{e}}$ be a complex eigenmode of the new hybrid algorithm (2) and assume that it has a growth factor $\rho$ such that $\mathbf{e}^{(n)} = \rho^n\tilde{\mathbf{e}}$. For this mode Eq. (2) gives

$$\sum_{k=1}^{K}\left(\mathbf{S}_k[\theta_k\rho^2 - (2\theta_k - 1)\rho + \theta_k] + \frac{1}{\Delta t^2}\mathbf{M}_k[\rho^2 - 2\rho + 1]\right)\tilde{\mathbf{e}} = 0. \tag{7}$$

Stability is equivalent to $|\rho| \le 1$ for all modes $\tilde{\mathbf{e}}$. With the substitution $\rho = (1+\zeta)/(1-\zeta)$ this condition becomes $\Re(\zeta) \le 0$, and (7) is transformed into

$$\sum_{k=1}^{K}\tilde{\mathbf{e}}^H\mathbf{S}_k\tilde{\mathbf{e}} = -\zeta^2\sum_{k=1}^{K}\tilde{\mathbf{e}}^H\left[\frac{4}{\Delta t^2}\mathbf{M}_k + \mathbf{S}_k(4\theta_k - 1)\right]\tilde{\mathbf{e}}. \tag{8}$$

Since all the matrices are Hermitian, $\zeta^2$ is real. Furthermore, since the left-hand side is nonnegative, stability follows if the sum on the right-hand side is positive for all $\tilde{\mathbf{e}}$. This sum can be split into the contribution from the explicit and implicit elements. The contribution from the implicit elements is nonnegative if $\theta_k \geq 1/4$ everywhere on this grid. By virtue of (6), the contribution from the explicit elements is nonnegative if the time step satisfies the CFL condition (5) for the FDTD. Therefore, the new implicit–explicit algorithm (2), with $\theta \geq 1/4$ on the implicit elements, is stable for time steps up to the stability limit of the FDTD.

Stability of a similar implicit–explicit hybrid in acoustics was proven by Belytschko and Mullen [15]. These authors used the trapezoidal integration rule in time on the implicit grid, with the displacement $\vec{\xi}$ and velocity $\vec{v} = \partial\vec{\xi}/\partial t$ placed on the same time levels. This is equivalent to the implicit scheme (1) with $\theta = 1/4$. An extensive overview over different time-stepping schemes used in computational mechanics, including explicit–implicit hybrids, is given by Hughes [16].

## 3. NUMERICAL RESULTS

One possible drawback of a hybrid method is reflections at the interfaces between the two types of grid. Here, we study such reflections for the new hybrid method and compare with our original scheme [8]. We also compare the hybrid to the FDTD with the staircase approximation for scattering from a perfect electrically conducting (PEC) sphere.

### 3.1. Reflection at Grid Interfaces

A simple arrangement to test the reflection at the FEM–FDTD interface is to inject a $TE_{10}$ mode into a waveguide. This is illustrated in Fig. 1, where a thin layer of tetrahedrons and pyramids is embedded in an FDTD grid of cubes. Figure 2 shows the cross section of the waveguide around the implicit layer for such a test. The width of the waveguide is twice its height.

The injected wave has the time dependence $E_y(t) = E_0 \exp[-(t - t_0)^2/d_0^2] \sin(2\pi f t)$, where $t_0 = 6.25/f_c$, $d_0 = 2.5/f_c$, $f = \sqrt{2} f_c$, and $f_c$ is the cutoff frequency for the $TE_{10}$ mode. The power reflection coefficients are shown as contour plots in Figs. 3a and 3b for the original and new hybrid scheme when the waveguide is discretized by $10 \times 5$ FDTD cells in the cross section.

The reflection for the new hybrid is much less sensitive to the choice of $\theta$ and $\Delta t$ than the original scheme. For the maximum FDTD time step and $\theta = 1/4$, the new hybrid gives a power reflection coefficient below $-46$ dB, while the original hybrid gives $-40$ dB.

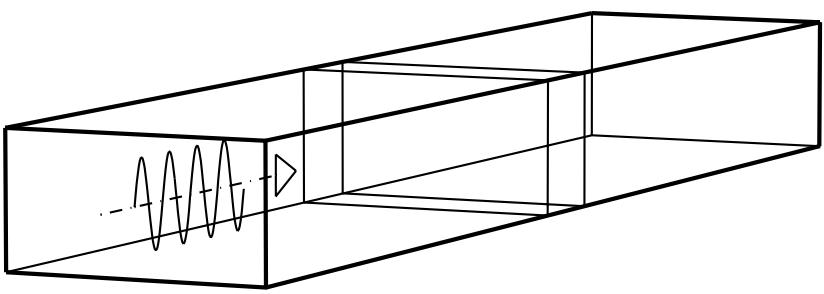

**FIG. 1.** Waveguide with the incident pulse traveling toward the implicit layer.

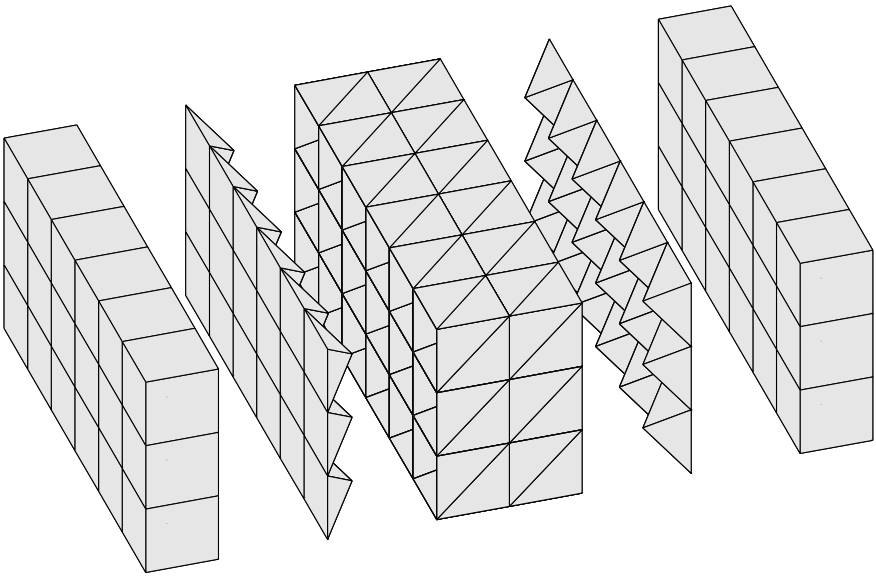

**FIG. 2.** Simple hybrid grid.

Riley [17] proposed another modification of the hybrid method, namely to apply trapezoidal integration over the bases of the pyramids. Figure 4 shows how the power reflection coefficient depends on resolution for $\theta = 1/4$, $\Delta t = \Delta t_{\mathrm{CFL}}$, and all four combinations of discretization techniques at the interface between the explicit and implicit grids. Here, the dimensions of the waveguide were kept fixed, while the thickness of the layer of tetrahedrons and pyramids was constant in numbers of cells. Results for the original and new

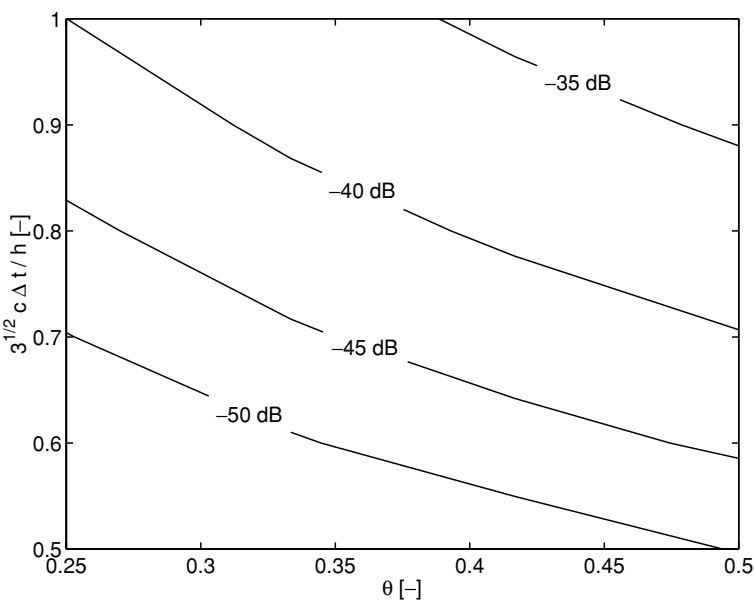


**FIG. 3a.** Level contours of the power reflection coefficient in the waveguide test for the original scheme with 14 cells per wavelength.

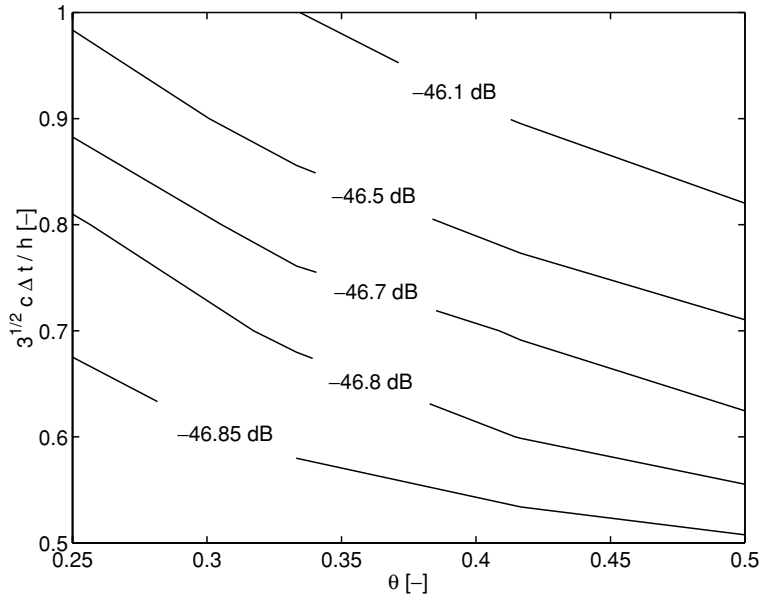


**FIG. 3b.** Level contours of the power reflection coefficient in the waveguide test for the new hybrid scheme with 14 cells per wavelength.

hybrid scheme are indicated by circles and squares, respectively, while dashed and solid lines correspond to exact and trapezoidal integration over the base of the pyramids, respectively. A least-squares fit to our results for $\lambda/h \geq 17$ shows that the power reflection coefficient varies as $h^{5.7}$.

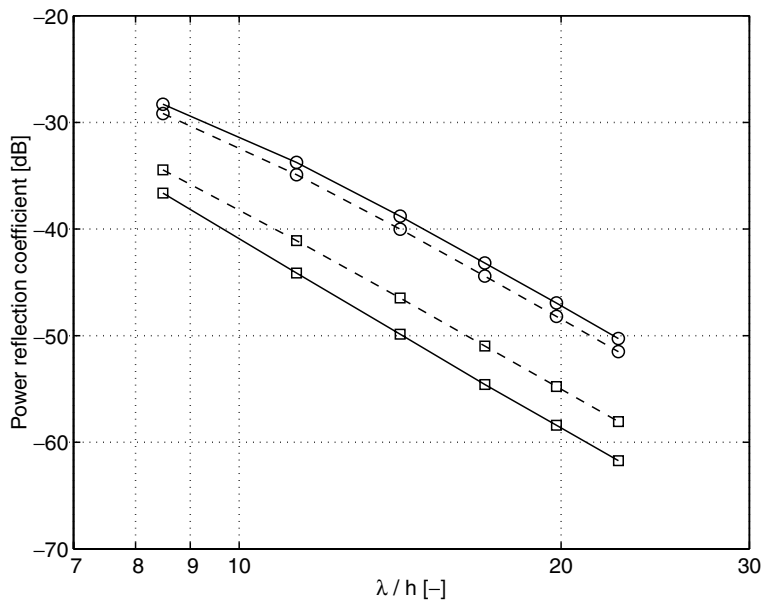


**FIG. 4.** Power reflection coefficient for $\theta = 1/4$ and $\Delta t = \Delta t_{\mathrm{CFL}}$ versus number of cells per wavelength. The new scheme is shown as squares, the original as circles. Dashed lines indicate exact integration over the pyramids, while solid lines indicate trapezoidal integration.

### 3.2. Scattering from PEC Sphere

We have also made tests comparing the hybrid to the FDTD for scattering by a PEC sphere. The hybrid was run with $\theta_k = 1/4$ on the tetrahedrons and pyramids and the time step at the CFL limit for the FDTD. The PETSc [18] sparse matrix package was used to solve the implicit equations in the FEM region. The inversion is done efficiently by the conjugate gradient method with a zero-fill-in ILU-preconditioner. The residual is reduced by about $10^{-6}$ with nine iterations.

An incident plane wave $E_{\text{inc}}(t) = E_0 \exp[-(t - t_0)^2/d_0^2] \sin[\omega_0(t - t_0)]$ is imposed at a Huygens surface [2]. The wavenumber vector of the incident plane wave is parallel to one of the Cartesian axes of the FDTD grid. The radiation pattern is obtained by means of a near-to-far-field (NTF) transformation [2]. We apply an NTF transformation using third-order Lagrange interpolation and four-point Gauss quadrature. It converges with an $O(h^4)$ error and gives a maximum error of 0.05% when $\lambda/h = 18$. The scattered wave is absorbed at the outer boundary by a "sponge layer" [19].

In [20], our original hybrid was validated with this setup against the analytic results for a PEC sphere. Here, we apply the same test to the new version. The bistatic RCS for a sphere of radius $a = 1$ m is computed on three different meshes with FDTD cell size $h = n/15\sqrt{3}$ m for $n = 9, 6$, and 4. The hybrid grids are constructed as described in [8] and parts of the grid for $n = 9$ are shown in Fig. 5. In this particular case, we generated tetrahedrons with edges of the length roughly equal to the corresponding FDTD cell size $h$. (For all resolutions, the average length of a tetrahedron edge is within 4% from $h$ and

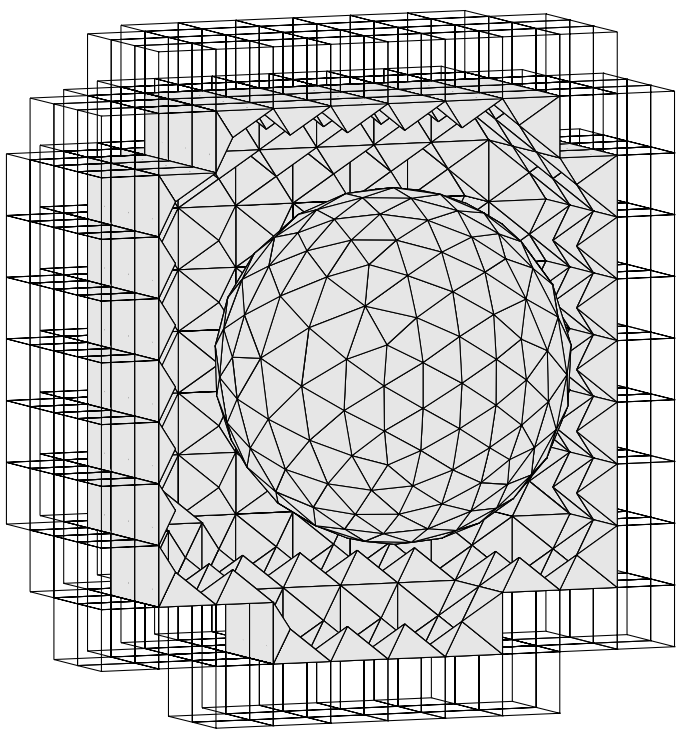

**FIG. 5.** Parts of the hybrid grid for the PEC sphere when $n = 9$. The discretized surface of the sphere is shown together with some of the pyramids. The first layer of FDTD cubes, connecting to the bases of the pyramids, is indicated by lines.

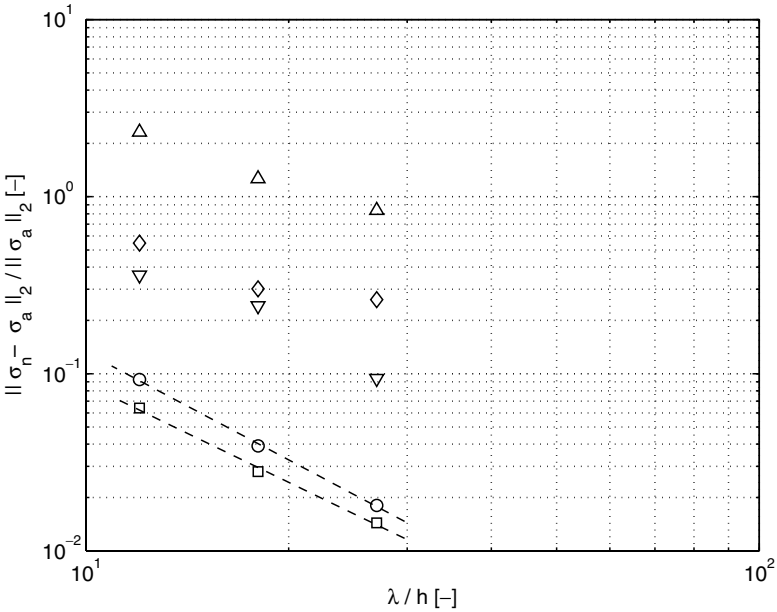


**FIG. 6.** The relative error in the bistatic RCS for a PEC sphere is shown by circles and squares for the original and the new hybrid scheme, respectively, and fits to the model $e(h) = ch^{\alpha}$ are shown by the dashed lines. For the staircased FDTD we used three different criteria for considering an FDTD cell PEC: (a) at least one corner of the cell was inside the physical sphere (△), (b) the midpoint of the cell was inside the physical sphere (◇), and (c) all corners of the cell were inside the physical sphere (▽).

the standard deviation is 20–23% of $h$.) Furthermore, we kept the thickness of the FEM grid constant in terms of cells when the resolution was increased and the average thickness was slightly below $2h$. Consequently, the fraction of the computational effort spent on the FEM region is proportional to $h$ for high resolutions. Although it is not needed for this particular test case, we emphasize that our hybrid allows local refinement of the FEM grid without reduction of the global time step. Such refinement can be necessary to resolve small geometrical details or the field in the vicinity of a singularity.

The wavelength is $\lambda = 4.16$ m ($ka = 1.5$) and the time constants are $t_0 = 1.73 \times 10^{-8}$ s, $d_0 = 6.00 \times 10^{-9}$ s. The relative error $e(h) = \|\sigma_n - \sigma_a\|_2 / \|\sigma_a\|_2$ is shown in Fig. 6 by circles and squares for the original and the new hybrid scheme, respectively, using exact integration for the pyramids. Here $\sigma_n$ and $\sigma_a$ are the numerically computed and analytic bistatic RCS, respectively, and $\| \cdot \|_2 = [\int_{\Omega} (\cdot)^2 \, d\Omega]^{1/2}$. The improved hybrid scheme reduces the error by 20–30% compared to the original version. With trapezoidal integration over the bases of the pyramids the relative error increased 2–3% for the original and 3–5% for the new hybrid scheme.

Least-squares fits to the model $e(h) = ch^{\alpha}$ are shown by the dashed lines in Fig. 6, and for the original and the new hybrid scheme we found $\alpha \simeq 2.02$ and 1.84, respectively. One effect that contributes to deviations from second-order convergence is the nonuniform refinement of the unstructured grid.

Table I shows the number of cells required for 5% accuracy in the bistatic RCS measured by the $L_2$ (rms) and $L_{\infty}$ (max) norms with the original and the improved hybrid scheme.

We applied this test to the staircased FDTD. Some rather arbitrary decisions have to be taken for the staircasing. Figure 6 shows results obtained using three different criteria for considering an FDTD cell PEC: (a) at least one corner of the cell is inside the physical

**TABLE I**
**Required Resolution $\lambda / h$ for 5% Accuracy in the Bistatic RCS for the PEC Sphere**

| 5% Accuracy | Original hybrid | Improved hybrid |
|---|---|---|
| In $L_2$-norm | 16.2 | 13.5 |
| In $L_\infty$-norm | 20.7 | 18.9 |

sphere ($\triangle$), (b) the midpoint of the cell is inside the physical sphere ($\diamond$), and (c) all corners of the cell are inside the physical sphere ($\triangledown$).

The errors for the staircased FDTD are about 5–60 times larger than those for the hybrid scheme. At all resolutions, the best FDTD result is obtained with method (c), where the FDTD cubes are modeled as conducting only when they are *completely* inside the sphere. This gives errors that are five to nine times larger than for the hybrid. To achieve a given relative error, the best FDTD (c) needs more than twice the linear resolution of the hybrid. Consequently, for the same accuracy as the FEM–FDTD hybrid method, the best FDTD (c) needs roughly 20 times more execution time and 10 times more memory. Moreover, the staircased FDTD schemes do not show a very clear order of convergence, which reduces the predictive power of extrapolation.

Table II shows the number of mega-floating-point operations (Mflops) per time step for the FDTD and FEM parts of the computation. Here, one flop is defined as one real number operation of the type multiplication, division, addition, or subtraction. The computational cost is almost six times higher for the sponge layer compared to the standard FDTD in homogeneous space, which is included in Table II. For the FEM part, the initial costs associated with the setup of the linear system of equations (computation of the element matrices excluded) and the computation of the preconditioner are amortized equally over all time steps. It should be mentioned that the total number of time steps is rather small for this particular problem, e.g., 206 time steps for $n = 9$, and that for all resolutions, the iterative solver used about 15 iterations for each time step. It is possible to reduce the flops per time step for the FEM part and keep sufficient accuracy. Note that the number of operations for the FEM region, relative to the FDTD region, decreases as the resolution increases and 10% of the flops are spent on the FEM part for the highest resolution, with 27 points per wavelength.

### 3.3. Scattering from the FEM–FDTD Interface

To investigate the scattering at the FEM–FDTD interface, we replaced the interior of the sphere by vacuum, discretized by tetrahedrons. The computed RCS of the empty grid

**TABLE II**
**The Number of Mega-Floating-Point Operations (Mflops) per Time Step for the FDTD and FEM Parts of the Computation**

| $15\sqrt{3}\,h$ | FDTD | FEM |
|---|---|---|
| 9 | 16 | 6.0 |
| 6 | 56 | 11 |
| 4 | 189 | 21 |

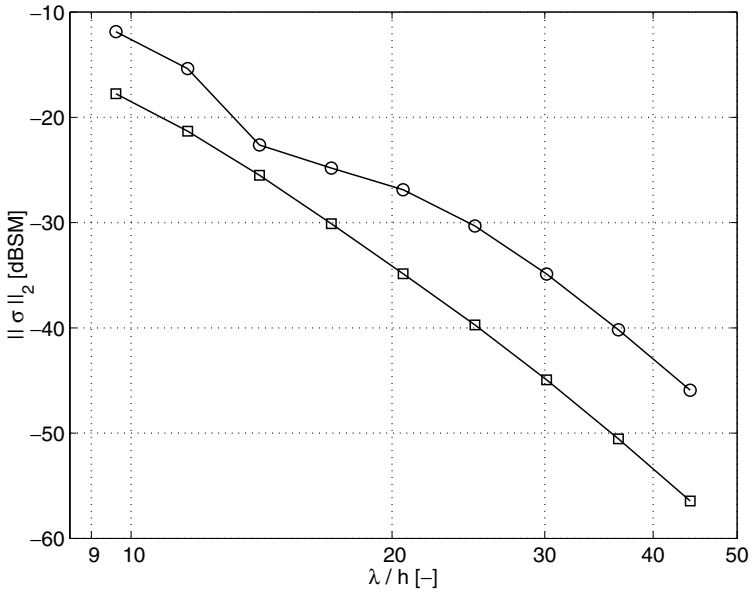


**FIG. 7.** The norm of the bistatic RCS for an empty sphere versus number of points per wavelength. Results for the new hybrid are shown as squares and for the original hybrid as circles.

is shown in Fig. 7 with respect to λ for different discretizations at the explicit–implicit interface. Here, the FDTD cell size is fixed to $h = \sqrt{3}/5$. (Since, in this figure, the quantity that varies is the wavelength, rather than the grid size, and the geometry is fixed, the result cannot be interpreted strictly as a convergence test.) The solid curves with circles and squares correspond to the original and the new scheme, respectively. Our new scheme for time stepping significantly reduces the scattering from the grid interface. According to Fig. 7, the improved hybrid reduces the RCS of the empty grid about 10 dB for $\lambda/h > 25$. For 12 cells per wavelength, the computed RCS of the empty grid was at least 35 dB below that of the conducting sphere in all directions. Trapezoidal integration over the bases of the pyramids changes the RCS of the empty grid less than 1 dB.

## 4. CONCLUSION

We have presented an improved version of the stable FEM–FDTD hybrid [8] and given a proof of stability for the new explicit–implicit time integration. The new hybrid reduces the reflection from the interface between the FEM and FDTD grids.

The standard FDTD scheme, with the staircase approximation, was compared with the hybrid for scattering from a PEC sphere. The hybrid converges toward the exact solution with an $O(h^2)$ error. For scattering from a conducting sphere with $ka = 1.5$ the hybrid achieves a root mean square accuracy of 5% with 13.5 cells per wavelength. For the FDTD, three different approaches for the staircasing gave significantly different results. The best FDTD results were obtained when only the cubes completely inside the physical sphere were modeled as conducting. This gave errors that were about five to nine times higher than for the hybrid scheme. With other choices for when to make an FDTD cell a conductor, the error could be as much as 60 times that of the hybrid. None of the tested staircasing strategies

for the FDTD produced a very clear order of convergence. To obtain results with accuracy comparable to the hybrid, the FDTD needs at least twice as many cells per wavelength as the hybrid. Since the number of the operations for the FEM part of the hybrid is typically less than for the FDTD part, the hybrid algorithm significantly reduces the total number of operations needed for a given accuracy.

We conclude that the hybrid method works robustly and combines the main advantages of the FDTD with those of edge finite elements on unstructured grids. In comparison to the staircased FDTD, the hybrid method is significantly more efficient when the geometry contains curved surfaces.

## ACKNOWLEDGMENTS

This work was supported in part by grants from the National Graduate School of Scientific Computing (NGSSC) and the Technical Research Foundation (TFR). The Center of Computational Electromagnetics is supported by the School of Electrical and Computer Engineering at Chalmers University. The research has profited in many ways from a collaboration with the Finite Element Center at Chalmers University.

## REFERENCES

1. K. S. Yee, Numerical solution of initial boundary value problems in isotropic media, *IEEE Trans. Antennas Propagat.* **14**, 302 (1966).
2. A. Taflove, *Computational Electrodynamics: The Finite-Difference Time-Domain Method* (Artech House, Norwood, MA, 1995).
3. J. Jin, *The Finite Element Method in Electromagnetics* (Wiley, New York, 1993).
4. J. C. Nédélec, Mixed finite elements in $R^3$, *Numer. Math.* **35**, 315 (1980).
5. K. S. Yee, J. S. Chen, and A. H. Chang, Numerical experiments on PEC boundary condition and late time growth involving the FDTD/FDTD and FDTD/FVTD hybrid, *IEEE Antennas Propagat. Soc. Int. Symp.* **1**, 624 (1995).
6. R. B. Wu and T. Itoh, Hybrid finite-difference time-domain modeling of curved surfaces using tetrahedral edge elements, *IEEE Trans. Antennas Propagat.* **45**, 1302 (1997).
7. A. Monorchio and R. Mittra, A hybrid finite-element finite-difference time-domain (FE/FDTD) technique for solving complex electromagnetic problems, *IEEE Microwave Guided Wave Lett.* **8**, 93 (1998).
8. T. Rylander and A. Bondeson, Stable FEM-FDTD hybrid method for Maxwell's equations, *Comput. Phys. Commun.* **125**, 75 (2000).
9. K. H. Dridi, J. S. Hesthaven, and A. Ditkowski, Staircase-free finite-difference time-domain formulation for general materials in complex geometries, *IEEE Trans. Antennas Propagat.* **49**, 749 (2001).
10. T. A. Driscoll and B. Fornberg, Block pseudospectral methods for Maxwell's equations. II: Two-dimensional, discontinuous-coefficient case, *SIAM J. Sci. Comput.* **21**, 1146 (1999).
11. P. Thoma and T. Weiland, Numerical stability of finite difference time domain methods, *IEEE Trans. Magn.* **34**, 2740 (1998).
12. R. Schuhmann and T. Weiland, Stability of the FDTD algorithm on nonorthogonal grids related to the spatial interpolation scheme, *IEEE Trans. Magn.* **34**, 2751 (1998).
13. M. Celuch-Marcysiak and W. K. Gwarek, Generalized TLM algorithms with controlled stability margin and their equivalence with finite-difference formulations for modified grids, *IEEE Trans. Microwave Theory Technol.* **43**, 2081 (1995).
14. J. F. Lee, R. Lee, and A. Cangellaris, Time-domain finite-element methods, *IEEE Trans. Antennas Propagat.* **45**, 430 (1997).
15. T. Belytschko and R. Mullen, Stability of explicit-implicit mesh partitions in time integration, *Int. J. Numer. Methods Eng.* **12**, 1575 (1978).

16. T. J. R. Hughes, *The Finite Element Method: Linear Static and Dynamic Finite Element Analysis* (Prentice-Hall, Englewood Cliffs, NJ, 1987).
17. D. J. Riley, Transient finite-elements for computational electromagnetics: Hybridization with finite differences, modeling thin wires and thin slots, and parallel processing, in *Applied Computational Electromagnetics Society (ACES) Symposium Digest, 17th Annual Review of Progress* (Monterey, CA, 2001) pp. 128–138.
18. S. Balay, W. D. Gropp, L. C. McInnes, and B. F. Smith, *PETSc Home Page*, available at `http://www.mcs.anl.gov/petsc` (1998).
19. P. G. Petropoulos, L. Zhao, and A. C. Cangellaris, A reflectionless sponge layer absorbing boundary condition for the solution of Maxwell's equations with high-order staggered finite difference schemes, *J. Comput. Phys.* **139**, 184 (1998), doi:10.1006/jcph.1997.5855.
20. T. Rylander and A. Bondeson, Application of stable FEM-FDTD hybrid to scattering problems, *IEEE Trans. Antennas Propagat.* **50**, 141 (2002).